ELSEVIER

Polymer 43 (2002) 909–919

polymer

www.elsevier.com/locate/polymer

Effects of mechanical interactions on the hydrostatic stress in randomly distributed rubber particles in an amorphous polymer matrix

Christophe Fond[1,*], Sébastien Géhant, Robert Schirrer

Institut Charles Sadron, 6, rue Boussingault, F67083 Strasbourg, France

Received 21 May 2001; received in revised form 29 August 2001; accepted 12 September 2001

Abstract

The equivalent inclusion method (EIM) assuming linear elasticity is used to calculate the mechanical interactions between spherical rubber particles in an amorphous matrix, as in a rubber toughened polymer. The influences of the various calculation parameters are examined and it is shown that the method can provide reliable results with regard to the level of hydrostatic stress in the particles. Damage of the material is simulated by replacing the most stressed particles by voids. Numerical simulations for several hundreds of interacting particles give information on the kinetics and spatial organisation of the damage. It appears that, as the volume fraction of particles increases from 10 to 20%, the spatial configuration of the damage evolves from a localised to a diffuse mode. These results are discussed in relation to the efficiency of rubber toughening.

Keywords: Rubber toughening; Mechanics; Interactions

1. Introduction

Although the rubber toughening of polymers is nowadays common practice [1] for many polymers, the behaviour at high strain rates still needs to be improved [2–4]. It is known that cavitation in the rubber particles constitutes an essential part of the mechanism of toughening [5,6] and it has been established that the residual brittleness of the amorphous polymer matrix can be due to an insufficient volume fraction of rubber. It is then thought that mechanical interactions between the rubber particles significantly modify the local stress fields and thus influence the way the material is damaged by cavitation [7]. Experiments have shown that cavitation precedes plasticity at high strain rates, owing to the increase of the matrix yield stress with increasing strain rate [8]. Hence one can assume that at high strain rates the elastic behaviour of the materials prevails and interactions between rubber particles are primarily responsible for the spatial organisation of the damage and its kinetics. Nevertheless, at very high strain rates such as those encountered at a crack tip during rapid crack propagation, the toughened material behaves as a glassy polymer and no whitening due to cavitation in the rubber particles is observed [9]. In this range of strain rates, or at temperatures close to or lower than the glassy transition temperature of the rubber, there is indeed less mechanical contrast between the elastic moduli of the matrix and the particles and this case will not be examined here.

Numerical simulations may be expected to inform us about the roles and synergy of various parameters, such as the volume fraction or cavitation criteria, in damage mechanisms. Therefore, we decided to perform some computations of the mechanical interactions between randomly distributed spherical rubber particles, in order to analyse the kinetics of damage and the spatial correlation of the damaged particles. It has been shown that cavitation is triggered by a critical hydrostatic stress in the rubber phase, the value of which could depend on the size of the rubber particle [10]. Moreover, owing to the elastic instability arising after cavitation [11,12], a damaged rubber particle behaves almost like a cavity. This allows us to simulate the damage process by simply replacing the damaged particles by spherical cavities in the computations. In practice, it is even possible to account for a low residual pressure acting at the particle–matrix interface after cavitation, for instance that induced by the surface tension in very small cavities, by lowering the Young's modulus of the rubber material in the particle, while keeping the Poisson's ratio unchanged to maintain a compressible fluid like behaviour inside the particle.

* Corresponding author. Tel.: +33-3-88-41-41-68; fax: +33-3-88-41-40-99.

E-mail addresses: fond@ics.u-strasbg.fr (C. Fond), schirrer@ics.u-strasbg.fr (R. Schirrer).

[1] http://www-ics.u-strasbg.fr.

0032-3861/02/$ - see front matter
PII: S0032-3861(01)00621-8

The equivalent inclusion method (EIM) has been shown to appropriately estimate the level of hydrostatic stress in spherical interacting rubber particles in an amorphous polymer matrix [13], assuming linear elasticity of both materials and for at least two particles. On the other hand, it has also been shown that the current formulation, based on a Taylor series development of the eigenstrains, is less appropriate to precisely evaluate the stress concentrations in the presence of strong interactions between heterogeneities. The mean value of the hydrostatic stress in the rubber particles is nevertheless expected to be precisely computed, even in the case of strong mechanical interactions, owing to the compressible fluid like behaviour of rubber materials under such solicitation. Moreover, calculations using a 0 order expansion, i.e. combining Eshelby's well known solutions [14,15], which have the characteristic that the stress fields are homogeneous inside a particle, are suitable to accurately estimate the mean hydrostatic stress. In a first approximation, the rubber material can in fact be regarded as a compressible fluid on account of its very low shear modulus to bulk modulus ratio. Consequently, the shear stress is negligible and the hydrostatic stress almost homogeneous [10]. The hydrostatic stress is in this case proportional to the volume variation of a rubber particle and therefore directly linked to the integral of the volume strain in the particle. This stress thus results from an average rather than a local value.

The following sections first describe the representative volume elements (RVE) and boundary conditions used in the numerical simulations. The reliability and accuracy of the method are then checked for various parameters of the computations. After having shown that the calculations give suitable estimates of the levels of hydrostatic stress in the rubber particles, the effect of the volume fraction of particles on the damage process is analysed. As the present analysis focuses on results provided by the EIM and for the sake of simplicity, the EIM is not presented in details herein and the reader is invited to refer for instance to Refs. [13,16,17].

2. Numerical simulation parameters

2.1. Construction of the representative volume elements

Since microscopic observations of the morphology of rubber toughened polymers generally do not show any particular spatial arrangement, we chose to randomly distribute the spherical rubber particles in the polymer matrix. In fact, as this random location was carried out by computer and hence inevitably perturbed by a logic, one should rigorously speak of a pseudo-random distribution. A description of the algorithm we used to generate the random numbers is given in numerical recipes [18].

A cubic volume of space is progressively filled with identical spheres until they occupy a given volume fraction of the cube. A cubic shape was chosen because it simplifies determination of the boundary conditions generated by the approximate solutions of the EIM. The coordinates of the centre of each sphere are randomly drawn, while ensuring there is no overlap with neighbouring particles. In non-periodic distributions, this filling procedure leads to a slightly higher volume fraction in the vicinity of the faces of the cube due to the absence of neighbours outside the cube. However, we found that this effect extends only over a distance equal to approximately three times the radius of a sphere. The volume we retained for the calculation of interactions was therefore a cube of size smaller than the initial volume where the spheres were distributed. A consequence of this procedure is that the volume fraction finally obtained is generally slightly lower than that initially expected. In periodic distributions there is of course no such effect.

2.2. Procedure for computation of the interactions

It is generally not possible to take into account all the particles in a single calculation. In the case of a group of particles spatially organised over a long distance, it would be best to include all the constitutive particles in the same interaction calculation, so that the more distant particles can interact through interposed neighbours. In practice, interaction computations are restricted to a spherical volume of radius D, centred on the particle for which the computation is currently being performed (Fig. 1). D represents the distance of effective interaction.

In order to avoid any border effect due to the absence of neighbouring particles, these calculations are only performed for particles located in a cubic volume of size at least $2D$ smaller than the cube where the spheres were initially distributed (dark grey particles in Fig. 1). This volume is assumed to be a representative volume element of the rubber toughened material. The eigenstrains of a particle located outside this RVE are determined by averaging the values obtained each time this particle is involved in a computation. If a particle has not been involved in any interaction computation, then it is assigned the mean values of the calculated eigenstrains for the particles in the RVE.[2] Once the eigenstrains are known for each particle, then it is possible to construct the stress and strain fields at any point in the cube by superimposing the effects of all the particles on the components of the fields applied at infinity [13,16]. Again, a distance must be chosen around each point for construction of the stress field. Since it is obvious that the stress at a given point is more strongly influenced by a close particle than a distant particle, relative to the size of these particles, it would seem consistent to use the same D value for construction of the stress field as for calculation of the interactions.

[2] Of course, considering a non-periodic case, one could say that particles not taken into account in any calculation appear to be inactive and hence useless since the same D value is used for computation of the unknown eigenstrains and for post-computation of the strain field.

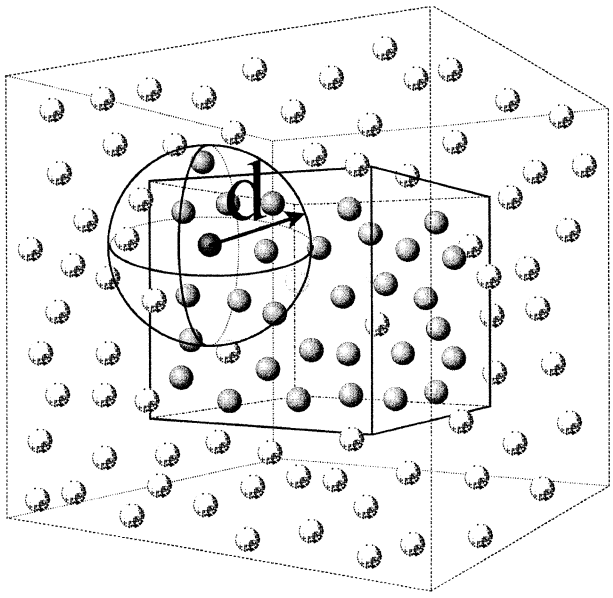

Fig. 1. Schematic RVE illustrating the differnet domains for computation of the interactions.

Periodic distributions are generated in cubic volumes in a classical way, so that a particle located just inside the RVE on one side is located just outside on the opposite side. As the distance of effective interaction is almost smaller than the RVE, computations for a periodic distribution will be called pseudo-periodic.

2.3. Boundary conditions

The stress/strain boundary conditions imposed on the cube constituting the RVE are evaluated after having computed the unknown eigenstrains and generally differ from those imposed at infinity. The remote strain tensor appears in the second equation of the linear system to be solved [13,16]. However, the reconstructed stress fields on the faces of the RVE have to be computed to determine the exact boundary conditions. A random distribution of spheres naturally ensures isotropic elastic behaviour for a sufficiently large cube and it has been verified that several hundred particles suffice to practically avoid anisotropy of the RVE. The displacements and normal and tangential stresses are numerically averaged at the surface of the RVE to calculate the mean applied strain and stress tensors. To obtain the desired stress boundary conditions on the faces of the RVE, three preliminary calculations are necessary to determine the remote strain to impose in the computation. In the objective of using available experimental data to validate or not the present results, the following boundary conditions relate exclusively to uniaxial tension.

2.4. Material characteristics

Typical elastic characteristics of a rubber toughened polymer are given in Table 1. A particularity of these materials resides in the strong contrast between the shear moduli of the particles and matrix, whereas their bulk moduli are similar. As far as we could see, the calculated tendencies are relatively insensitive to small variations of these moduli, so long as this contrast remains important. The sensitivity to these parameters is for simplicity not presented here. Using the values of Table 1, Eshelby's solution predicts the hydrostatic stress in a spherical rubber particle to be $P_{h0} = 0.7647\mathrm{Tr}(\sigma)/3$, where σ is the remote stress tensor. One notes that this solution assumes the absence of interactions (one particle in an infinite medium) and linear elastic behaviour of the two phases and is such that the stress field is uniform in any ellipsoidal particle.

3. Assessment of the technique

3.1. Homogenised elastic moduli

A simple way to globally check the quality of the solution provided by the EIM is to consider the homogenised elastic moduli of the RVE. Although this method of calculation was chosen to obtain information about the local stress fields, the homogenised elastic moduli are the least one can expect from the results. Indeed, the interest of this method for studies of cavitation damage lies in a knowledge of the relative values of the hydrostatic stress in particles, more than its absolute values. Since the approximate solution is a superposition of cinematically admissible fields, the calculated elastic energy is expected to be always greater than that corresponding to the exact solution. This is due to the parasitic work resulting from stress discontinuities at the interfaces, the approximate stress field being statically inadmissible. Let us note, for an easier understanding, that the solution provided by the EIM is approximate for the boundary conditions imposed, here homogeneous, but exact for the boundary conditions reconstructed from the eigenstrains, conditions which include the stress discontinuities at the interfaces.

Fig. 2 shows the results obtained using three classical models, the Voigt and Reuss and Hashin and Shtrikman [19,20] boundary models and the two phase self-consistent model. As expected, the present numerical simulations give

Table 1
Elastic moduli used in the numerical simulations

	Young's modulus	Poisson's ratio	Bulk modulus	Shear modulus
Particles	$E_n = 1$ MPa	$\nu_n = 0.49985$	$K_n = 1.11$ GPa	$\mu_n = 333.3$ kPa
Matrix	$E_m = 2$ GPa	$\nu_m = 0.35$	$K_m = 2.22$ GPa	$\mu_m = 740.7$ MPa

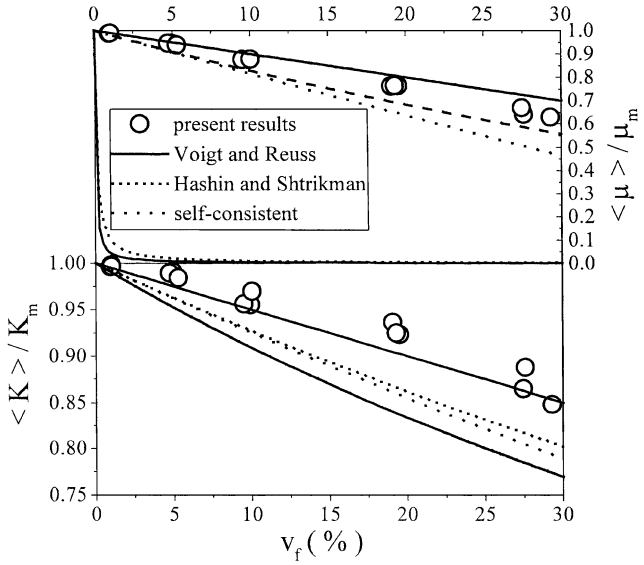

Fig. 2. Comparison of homogenised elastic moduli obtained by numerical simulations taking into account the mechanical interactions with three of the most commonly employed homogenisation models. $\langle K\rangle$ and $\langle\mu\rangle$ denotes, respectively, the homogenised bulk and shear moduli, K_m and μ_m denotes, respectively, the matrix bulk and shear moduli.

high homogenised moduli, which are nevertheless relatively close to the upper boundary of Hashin and Shtrikman for all volume fractions. The number of strong interactions increases with increasing volume fraction. It is difficult to rigorously assess the ability of the method to provide an accurate result, though one may note that the estimations of the EIM do not seem to degrade as the volume fraction rises. Hence the EIM does not diverge as the number of strong interactions increases.

A more precise analysis can be performed with the finite element method (FEM), since it allows the modelling of infinite periodic media. Although the EIM is not valid for such media, these can still be approached by considering lattices which contain a finite, but sufficiently large number of particles. In Fig. 3, the hydrostatic stresses computed by

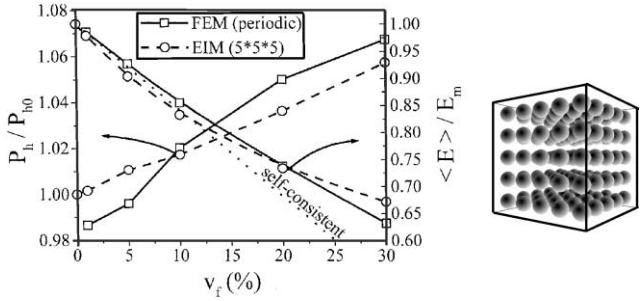

Fig. 3. Comparison of the mean hydrostatic stresses, P_h, and homogenised Young's moduli, $\langle E\rangle$, deduced from FEM and EIM computations, for particles forming a periodic medium with cubic symmetry. Right: representation of the RVE, containing 125 particles, used for the EIM computations. v_f denotes the volume fraction of particles. P_{h0} denotes the hydrostatic stress for a single particle in an infinite matrix in which Young's modulus is E_m.

the EIM in the central particle of a cubic array of $5\times5\times5$ particles are compared to those obtained with the FEM in a cubic symmetry, for volume fractions ranging from 0 to 30%. The corresponding homogenised Young's moduli under uniaxial tension are compared on the same figure. The two solutions are in good agreement and the EIM provides results in the range of accuracy of the FEM. One notes in addition that the EIM solution is exact for volume fractions close to 0%. Concerning the elastic moduli, the maximum deviation from the predicted Poisson's ratio is less than 1.4%. Since the FEM results at low volume fractions are close to the expected values, we can assume that the FEM model is reliable, and hence likewise the EIM at higher volume fractions. Owing to the mechanical interactions induced by this particular periodicity, the Young's modulus predicted by the self-consistent model differs significantly from that of the numerical simulations for volume fractions of particles greater than approximately 15%.

In order to further normalise the results according to the volume fraction of particles, the mean expected hydrostatic stresses in the rubber particles P_{h0} may be estimated with a two phase self-consistent model, i.e. by inserting the elastic moduli of Fig. 2 into Eshelby's solution. This leads to the relation:

$$P_{h0}(v_f) \approx (0.7647 + 0.2436v_f + 0.1622v_f^2)\mathrm{Tr}(\sigma)/3 \qquad (1)$$

where v_f is the volume fraction of rubber particles in the range 0–30%. The variation of P_{h0} with v_f is due to the variation of the homogenised moduli of the material surrounding the particles. Thus for example, the strain boundary conditions being set, the required strain to obtain a given stress increases as the Young's modulus of the material decreases. This explains a positive carry-over of hydrostatic stresses in the rubber particles for randomly interacting particles, in contrast to Eshelby's model which assumes non-interacting particles.

3.2. Influence of the computation parameters on the hydrostatic stress distribution in particles

3.2.1. Order of expansion of the eigenstrains

In the presence of mechanical interactions, the hydrostatic stress in the rubber particles varies from one particle to another and the proximity of other particles in fact significantly influences cavitation [21]. It is expected that the poorest results will be obtained for the highest volume fractions of particles which lead to the strongest interactions. Fig. 4 compares calculations using zero and first order expansions for pseudo-periodic and non-periodic RVE with $v_f \approx 30\%$. The distributions are almost identical for the two populations and the two orders of expansion. Whatever the parameters of computation, the pseudo-periodic and non-periodic RVE give similar results, while the variation between the maximum values of the average hydrostatic stress for these four calculations does not exceed

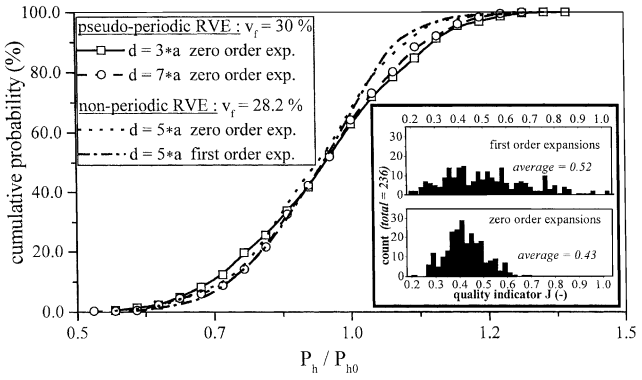

Fig. 4. Influence of the distance of effective interaction and the order of Taylor's expansions on the distribution of the hydrostatic stress, P_h, in rubber particles, for particle volume fractions of approximately 30%, in a pseudo-periodic and a non-periodic medium. P_{h0} is the self-consistent estimate of the mean hydrostatic stress given by Eq. (1). The distributions of the quality indicator, J, of the solutions are given in the insert (see Appendix A).

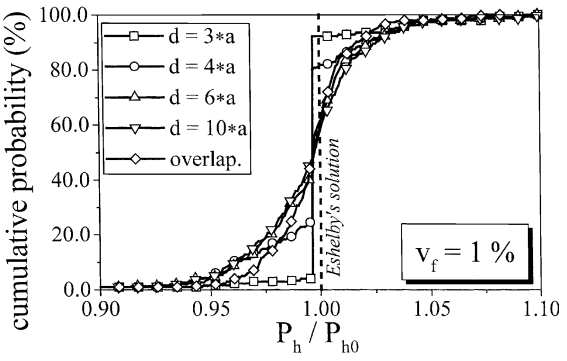

Fig. 6. Influence of the distance of effective interaction on the distribution of the hydrostatic stress, P_h, in rubber particles for a volume fraction of 1%. The values are derived from computations using zero order expansions, or in one case by simple overlapping of the elastic fields corresponding to single particles in an infinite medium. P_{h0} is the self-consistent estimate of the mean hydrostatic stress given by Eq. (1). d is the distance of effective interaction, a the radii of the particles and v_f the volume fraction of particles.

2%. These results therefore seem to be only slightly sensitive to the order of expansion. As the average values are very close to those of P_{h0} in Eq. (1), one may deduce that shielding effects compensate for the stress concentrations due to interactions.

The quality criterion J, a quantity proposed by Fond et al. [13] and based on the stress discontinuities at the interface of each heterogeneity, ranges from 0.2 to 0.7 for the zero order expansions. These values may be compared with those obtained for two particles under uniaxial tension, where exact solutions are known [13]. In this particular configuration, J is equal to about 0.3 for an error of the mean hydrostatic stress of less than 2% (Fig. 5). Since the value of the quality criterion J is closely related to the stress discontinuities, we can expect it to increase with the number and proximity of neighbouring particles. The range of values obtained for randomly distributed particles in this respect gives confidence in the predicted results.

It is noticeable that first order calculations, although much more time consuming, generally do not offer better results than zero order calculations, with regard to the hydrostatic stress. Moreover, the J distributions of first order expansions are broader than those of zero order expansions and there is indeed no reason for the present formulation of the EIM to converge with increasing order of expansion [13]. Since rubber behaves like a compressible fluid, use of zero order calculations would thus seem to be more appropriate to determine the hydrostatic stress in randomly distributed rubber particles, as this forces the stress field to be almost uniform in the particles.

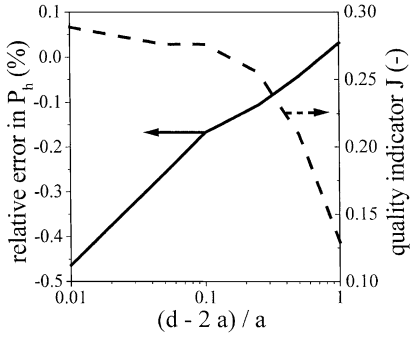

Fig. 5. Correlation between the quality indicators and accuracy of the computations for two rubber particles aligned along the tensile axis. The relative error in P_h is obtained by comparing values from the EIM with exact values given in Ref. [13]. The J quantity, based on the stress jump at the particle/matrix interface, is defined in Appendix A.

3.2.2. Distance of effective interaction

Fig. 6 shows the influence on the hydrostatic stress distribution of the chosen distance of effective interaction D for a 1% volume fraction of particles. In such a dilute medium, only a few particles can interact with their neighbours when D is smaller than about 3 times the radius of a particle. Hence initially almost all particles exhibit a hydrostatic stress equal to that of a single particle in an infinite medium. As the distance D increases, more and more particles interact with their neighbours and the distribution broadens. However, beyond a distance of effective interaction equal to about five times the radius of a particle, the shape of the distribution for a given population of particles ceases to evolve with further increase in D. This suggests that each particle interacts only with its closest neighbours, which tend to screen out the influence of more distant ones. The same tendency was also observed at higher volume fractions, but for shorter distances D (Fig. 7).

Also presented in Figs. 6 and 7 are the results obtained by simple superposition of the perturbation fields generated by the particles, assuming the eigenstrains to be those of Eshelby's solution (non-interacting particles). This straightforward method, which does not require the solution of a system of equations but does not really take into account

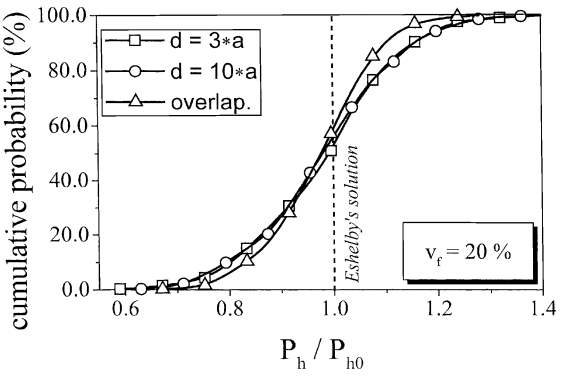

Fig. 7. Influence of the distance of effective interaction on the distribution of the hydrostatic stress in rubber particles for a volume fraction of 20%. The values are derived from two computations using zero order expansions and one based on simple overlapping of the elastic fields corresponding to single particles in an infinite medium. P_{h0} is the self-consistent estimate of the mean hydrostatic stress given by Eq. (1). d is the distance of effective interaction, a the radii of the particles and v_f the volume fraction of particles.

interactions, gives tendencies similar to those of the EIM with as expected slightly narrower distributions of the hydrostatic stress. Since our objective was to accurately determine the higher stresses in rubber particles in order to study the spatial organisation of the cavitation in the early stages of damage, we preferred the EIM. Nevertheless, a comparison of these two methods is of interest. In fact, whereas it cannot be proved that the EIM does not diverge with increasing volume fraction of the particles, there is no reason for the overlapping method to diverge with increasing volume fraction. Once again, the fact that the tendencies are the same gives confidence in the calculated results.

At $v_f = 1\%$ the average hydrostatic stress in the particles lies within $\pm 0.5\%$ of the estimate of Eq. (1) and at $v_f = 20\%$ within $\pm 0.7\%$ of this estimate. Concerning particle interactions, this would appear to confirm that shielding compensates the stress concentration effects. However, the EIM is not sufficiently accurate to explain more precisely the origin of the slight differences between the computed mean values and those estimated from Eq. (1).

3.3. Conclusions concerning the computational method

In summary, zero order expansions of the numerical simulations seem to be adequate to evaluate the distribution of hydrostatic stress in rubber particles, while periodic and pseudo-periodic computations give results analogous to those obtained for non-periodic populations. Variation of the distance of effective interaction shows that beyond a certain value, which depends on the volume fraction of particles, the distribution does not evolve further. The accuracy of the method, with regard to the hydrostatic stress inside the particles, cannot be checked with exact solutions for several hundreds of particles, but all tests we performed led us to believe that this accuracy is of the order of a few percent.

4. Evolution of the damage in rubber toughened polymers

4.1. Distribution of the hydrostatic stress in particles

Fig. 8 illustrates the influence of the volume fraction of particles v_f on the distribution of the hydrostatic stress in particles. As expected, the distributions are broader for higher volume fractions, while the average values always lie close to the estimate of Eq. (1). This indicates that assuming linear elasticity, the cavitation process will be more progressive for high than for low volume fractions of particles. The prediction is consistent with many experimental observations which show that a volume fraction of at least 15% is typically required for efficient toughening of polymers with pure rubber particles.

4.2. Cavitation model and normalisation of results

As mentioned in Section 1, it is now generally accepted that the level of hydrostatic stress in the particles is the key parameter triggering cavitation. Our model supposes that all particles have the same resistance to cavitation and that the most stressed particle in the RVE, with respect to the mean positive hydrostatic stress, undergoes cavitation. Once this most stressed particle has been determined, any other particle located outside the RVE and presenting an equal or higher internal hydrostatic stress is considered to have cavitated too. A new interaction computation can then be carried out, in which the mechanical characteristics of all the cavitated particles are replaced by those of a damaged particle. When replacing these particles by cavities, the model treats the extreme case of soft rubbers, where the interface tractions after cavitation are negligible for particles typically larger than 100 nm, owing to the elastic instability related to cavitation and the small effect of surface tension inside the cavities [10]. Calculations were

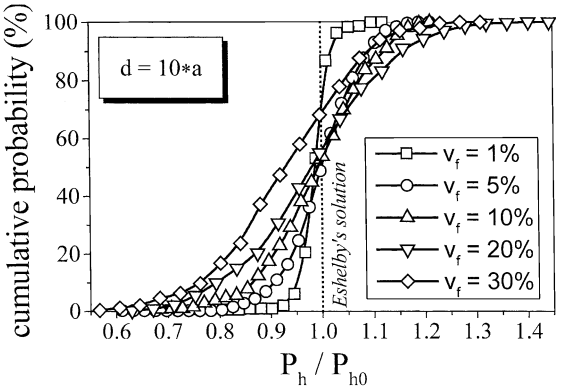

Fig. 8. Influence of the volume fraction of rubber particles on the distribution of the hydrostatic stress in particles for computations using zero order expansions and a distance of effective interaction equal to ten times the radius of a particle. P_{h0} is the self-consistent estimate of the mean hydrostatic stress given by Eq. (1). d is the distance of effective interaction, a the radii of the particles and v_f the volume fraction of particles.

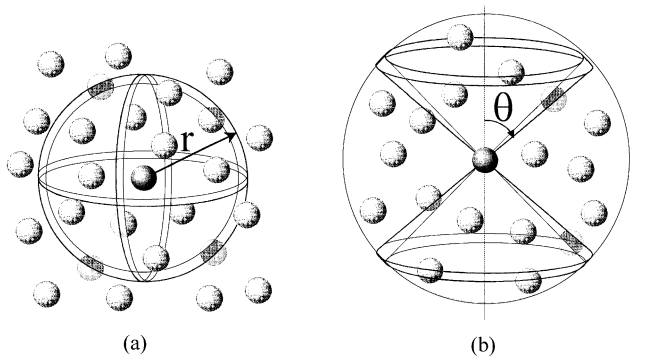

Fig. 9. Schematic representation of an analysis of the geometrical correlation between the positions of cavitated particles, as a function of: (a) the distance r and (b) the angle θ with the tensile direction.

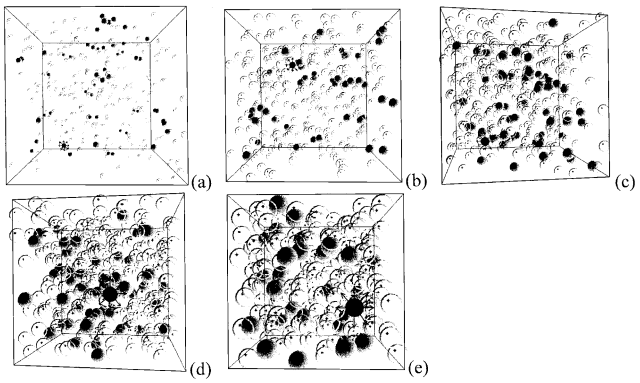

Fig. 10. Visualisation of the damaged particles (grey) among the non-damaged particles (transparent) for 15% damaged particles and volume fractions of (a) 1%, (b) 5%, (c) 10%, (d) 20% and (e) 30%, under uniaxial tension. The last damaged particle is represented by the symbol  .

carried out at zero order with $D = 5a$, where a is the radius of a particle. The boundary conditions were revised at each iteration to ensure that the RVE remained under pure uniaxial tension.

The spatial organisation of the cavitation was characterised by letting each cavitated or non-cavitated particle give rise to a radial and angular analysis of its neighbourhood, as schematised in Fig. 9. Once again, the distance of effective interaction D was used to select only the closest neighbours in the angular analysis. Averaging of the results over all particles involved allowed eight functions to be constructed at each iteration of the computations:

$C(r/a)$ and $C_{nn}(\theta)$, representing, respectively, the probability of finding any particle at a distance r/a from the centre of any other particle, or in a direction forming an angle θ with respect to the tensile direction.
$C_{nd}(r/a)$ and $C_{nd}(\theta)$, representing respectively the probability of finding a damaged particle at a distance r/a from the centre of any particle, or in a direction forming an angle θ with respect to the tensile direction.
$C_{nd}(r/a)$ and $C_{nd}(\theta)$, representing, respectively, the probability of finding any particle at a distance r/a from the centre of a damaged particle, or in a direction forming an angle θ with respect to the tensile direction.
$C_{dd}(r/a)$ and $C_{dd}(\theta)$, representing, respectively, the probability of finding a damaged particle at a distance r/a from the centre of another damaged particle, or in a direction forming an angle θ with respect to the tensile direction.

4.3. Spatial organisation of the damage

Fig. 10 depicts, for five different RVE and particle volume fractions of 1, 5, 10, 20 and 30%, the spatial organisation of the damage when 15% of the particles are damaged under uniaxial tension. It appears that for volume fractions of up to 10%, the damaged particles tend to be arranged in clusters, which are mostly oriented in planes perpendicular to the direction of traction. At volume fractions of 20 and 30% this organisation tends to disappear.

Statistical analyses were performed to characterise more objectively the organisation and progress of cavitation and Fig. 11 shows typical results for a 5% particle volume fraction. The shape of the curves for $r/a \approx 1$ is due to spatial obstruction by the particle in question. The higher probability of finding a particle close to a damaged one indicates that the particle interactions favour cavitation in clusters. This effect is very marked at the beginning of the damage and progressively disappears for obvious reasons as the proportion of damaged particles increases. The interactions also favour cavitation in planes perpendicular to the tensile direction ($\theta \approx 90°$), particularly for low volume fractions of damaged particles. The maximum at approximately 70° is related to the randomness of the population and the relatively limited number of particles included in the simulation. Finally, the evolution of the spatial correlation for different volume fractions, presented in Fig. 12 for a 13% fraction of damaged particles, shows clearly that the tendency to spatial organisation decreases as the volume fraction of particles increases.

5. Discussions

No proof of the convergence of the EIM has been proposed to date and there exist only a few reference solutions for this kind of analysis. Nevertheless, an evaluation of the precision of our calculations using the quality indicator of Fond et al. [13] allows us to consider that the method gives reliable values for the hydrostatic stress in rubber particles. As a result of the kinematic admissibility of the approximate solutions of the EIM, the homogenised elastic moduli are always over-estimated. One might suppose that this would lead to a slight shift of the mean values of the hydrostatic stress in particles, but the averages obtained are in good agreement with models of the self-consistent type. Moreover, the interest of this method for studies of cavitation damage lies in a knowledge of the relative values of the hydrostatic stress in particles, more than its absolute values.

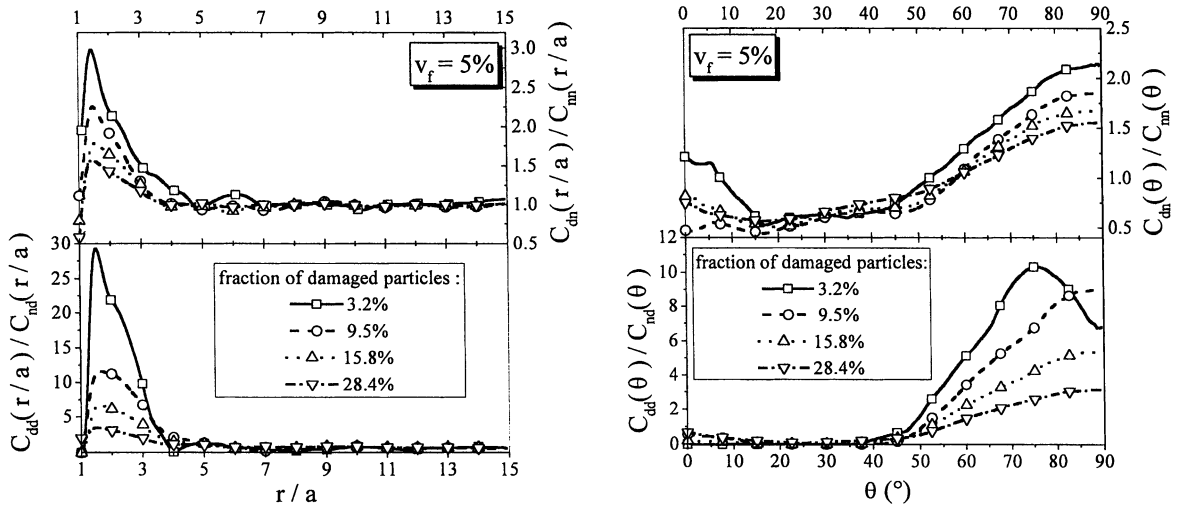

Fig. 11. Effect of the interactions between particles on the cavitation mechanism: statistical analysis illustrating the proximity and angular correlations of cavitation for a 5% volume fraction of particles. The quantities C_{dd}, C_{nd}, C_{dn}, and C_{nn} are defined in Section 4.2.

The distribution of the hydrostatic stress in particles reflects a strong influence of the volume fraction of particles. At low volume fractions, the damage process favours the formation of clusters of cavitated particles, which behave like pseudo-crazes and weaken the material. Conversely, the progressive nature of the damage could constitute one of the elements responsible for rubber toughening at high volume fractions. A typical evolution of the number of damaged particles as a function of the applied stress is shown in Fig. 13. Since the overall curves are monotonously increasing, there is no evidence of any avalanche effect, within the accuracy of the computations. A fortiori, no avalanche effect is to be expected in the presence of dissipation in the matrix, i.e. viscoelasticity, plasticity or viscoplasticity.

The chronology of the particle damage is more sensitive to the relative positions of the particles than to their state, i.e. whether they have cavitated or not. Thus, numerical simulations carried out by damaging the five most stressed particles in the RVE at each iteration presented a chronology of cavitation almost identical to those in which the particles were damaged one by one. Furthermore, it was found that the cavitation sequence could be almost deduced from the hydrostatic stress distribution obtained before damage of any particle. Hence the cavitation of a particle does not strongly affect the local interactions with its neighbours.

6. Conclusions

Since at high strain rates or low temperatures, the elastic behaviour can be uncoupled from viscosity and plasticity, it

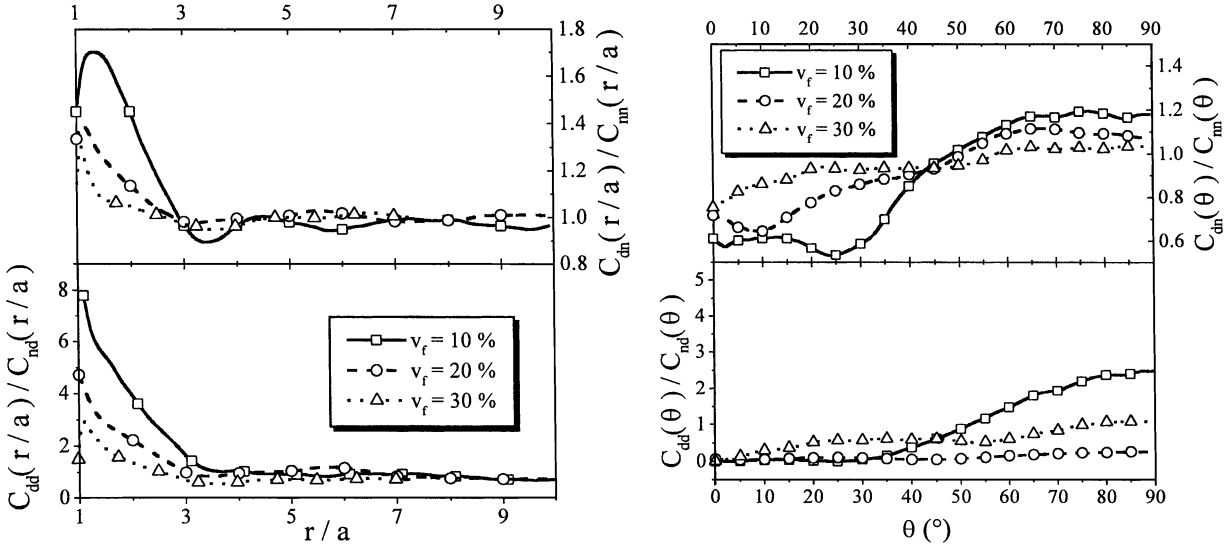

Fig. 12. Effect of the interactions between particles on the cavitation mechanism: statistical analysis illustrating the proximity and angular correlations of cavitation for 13% damaged particles. The quantities C_{dd}, C_{nd}, C_{dn}, and C_{nn} are defined in Section 4.2.

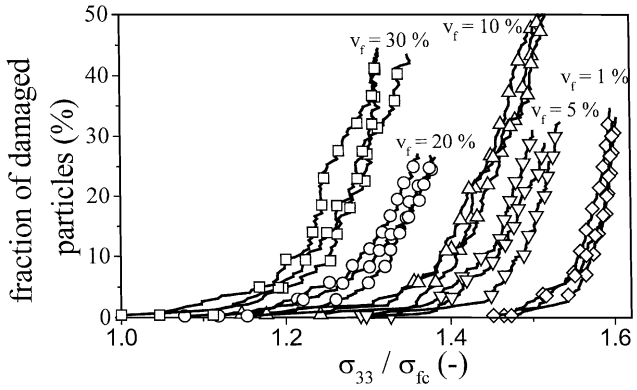

Fig. 13. Evolution of the fraction of damaged particles with the macroscopic stress σ_{33} for various volume fractions and under uniaxial tension (σ_{fc} is chosen arbitrarily to be the stress for which the first cavitation occurs). v_f denotes the volume fraction of particles.

is possible to highlight the influence of the volume fraction of rubber particles on the distribution of the hydrostatic stress in particles and the kinetics of cavitation by means of the present numerical simulations. The diffuse nature of the damage for volume fractions of over 20% could have a shielding effect on the propagation of cracks and crazes. Microscopic observations indeed reveal that cavitated particles can constitute sites of attraction which stop crazes [3] and rubber toughening is then more effective as it deviates the paths of the crazes.

On the other hand, the presence of a sufficient volume fraction of particles significantly lowers the macroscopic yield stress, owing to the stress concentrations at the particle–matrix interfaces. At low macroscopic stress, the local energy density is low and thus the energy release rates associated with the propagation of micro-crazes are likewise low. This could influence the competition between the genesis, propagation and coalescence of crazes and the formation of dilatational bands. Such competition could explain very simply the ductile–brittle transition related to changes in the volume fraction of rubber toughening particles. It is unfortunately not possible to use the current form of the EIM to study the competition between cavitation in the rubber particles and the formation of crazes or shear bands, since this requires a more precise evaluation of the stress concentrations at the particle–matrix interfaces. Nevertheless, a way of improving the interaction computations by using variational principles has been proposed by Fond and Gilormini [22]. To be able to further examine this question, it will be necessary to have tools which take into account the non-linear behaviour of the phases, or at least of the matrix. Some methods of analysis have been put forward recently, as for example by Ref. [23], for these kinds of morphology and behaviour, but the number of heterogeneities must still be reduced in accordance with the capacity of present day computers.

Finally, in a random distribution the probability of encountering spheres organised in space, for instance aligned in a plane, on a large scale is low, since one considers a relatively small number of particles, typically a few thousand in our numerical simulations. Consequently, it is not certain that our conclusions still hold for such rare geometrical configurations.

Appendix A

A.1. The equivalent inclusion method principle

An inclusion is a domain of the matrix which is subjected to a stress free strain, also called eigenstrain, in other words, a thermal dilatation, plastic strain or phase transformation strain which would not induce any stress in the inclusion if it were not embedded in a matrix. An inhomogeneity is a domain with elastic constants different from those of the matrix. Stresses arise from incompatibility of the deformation between the inclusion and the surrounding matrix, assuming perfect adhesion at the inclusion–matrix interface. 'Eigenstress fields are created by the incompatibility of eigenstrains.'

The EIM has been described in detail elsewhere [13–17] and only a brief summary will be given below. Bold characters denote tensors and vectors and *italics exact functions*. For the sake of clarity, the eigenstrain tensors B^p take values in the pth inclusion and are zero outside. The general equivalence equation is then:

$$\mathbf{C}^p(\mathbf{x})\left(\varepsilon^0(\mathbf{x}) + \sum_{q=1}^{N} D^q(\mathbf{x}-\mathbf{x}_q)B^q(\mathbf{x})\right) = C^0\left(\varepsilon^0(\mathbf{x}) + \sum_{q=1}^{N} D^q(\mathbf{x}-\mathbf{x}_q)B^q(\mathbf{x}) - B^p(\mathbf{x})\right) \quad \text{(A1.1)}$$

for every point $\mathbf{x} = (x, y, z)$ inside an inhomogeneity (left hand side) or inclusion (right hand side), where N is the number of inclusions and $\mathbf{x}_q = (x_q, y_q, z_q)$ the centre of the qth inclusion. D^p is a fourth order tensor representing the influence functions, which are the effects of B^p on the strains at point $\mathbf{x}$. $\varepsilon^0(\mathbf{x})$ denotes the remote strain tensor, the strain which would prevail in the absence of an inhomogeneity. $\mathbf{C}^p$ and $\mathbf{C}^0$ are the stiffness tensors of the pth inhomogeneity and the matrix, respectively, and for our purposes $\mathbf{C}^p$ is assumed to be uniform in the inhomogeneities.

In order to use analytical solutions, the eigenstrain B_j^p is approximated by a Taylor series, which for numerical calculations must be truncated to the order T. The subscript j refers to the component of the strain tensor, using the reduced indices $(11 \rightarrow 1, 22 \rightarrow 2, 33 \rightarrow 3, 23 \rightarrow 4, 13 \rightarrow 5, 12 \rightarrow 6)$. This leads us to define the eigenstrain tensors $\boldsymbol{\beta}^p(a,b,c)$ as follows:

$$B_j^p(\mathbf{x}) \approx \sum_{a,b,c}^{0\le a+b+c\le T} \boldsymbol{\beta}_j^p(a,b,c)(x-x_p)^a(y-y_p)^b(z-z_p)^c \quad \text{(A1.2)}$$

where a, b and c are positive integers or zero such that $0 \leq a+b+c \leq T$. The remote strain is approximated in the same way by a Taylor series and it should be noted that the remote strain field $\boldsymbol{\varepsilon}^0$ can be non-uniform:

$$\boldsymbol{\varepsilon}_j^{0p}(\mathbf{x}) \approx \sum_{a,b,c}^{0\leq a+b+c\leq T} \boldsymbol{\epsilon}_j^{0p}(a,b,c)(x-x_p)^a(y-y_p)^b(z-z_p)^c \tag{A1.3}$$

If a uniform strain field is applied at infinity, $\boldsymbol{\epsilon}_j^{0p}(a,b,c)$ vanishes whenever $a+b+c \neq 0$. The equivalence equation may then be rewritten:

$$\begin{aligned}
&\sum_{a',b',c'}^{0\leq a'+b'+c'\leq T} \mathbf{C}^p(\mathbf{x})\Bigg[\boldsymbol{\epsilon}^{0p}(a,b,c)(\mathbf{x}) \\
&\quad + \sum_{q=1}^{N} D^q(a',b',c')(\mathbf{x}-\mathbf{x}_q)\boldsymbol{\beta}^q(a',b',c')\Bigg] \\
&\approx \sum_{a',b',c'}^{0\leq a'+b'+c'\leq T} \mathbf{C}^0\Bigg[\boldsymbol{\epsilon}^{0p}(a,b,c)(\mathbf{x}) \\
&\quad + \sum_{q=1}^{N} D^q(a',b',c')(\mathbf{x}-\mathbf{x}_q)\boldsymbol{\beta}^q(a',b',c') - \boldsymbol{\beta}^p(a,b,c)(\mathbf{x})\Bigg]
\end{aligned} \tag{A1.4}$$

for all (a, b, c). The tensors $D^q(a',b',c')$ are analytically known. However, as Eq. (A1.4) cannot generally be solved analytically, $D^q(a',b',c')$ must also be approximated by a Taylor series in order to obtain a linear system of equations. This leads us to define the fourth order tensor $\mathbf{D}_{jk}^{pq}(a,b,c,a',b',c')$ as follows:

$$\begin{aligned}
&\mathbf{D}_{jk}^{pq}(a,b,c,a',b',c')\boldsymbol{\beta}_k^q(a',b',c') \\
&\quad \approx \frac{1}{a!b!c!}\frac{\partial^a}{\partial x^a}\frac{\partial^b}{\partial y^b}\frac{\partial^c}{\partial z^c} D_{jk}^q(\mathbf{x}-\mathbf{x}_q)_{|\mathbf{x}_p}\boldsymbol{\beta}_k^q(a',b',c')
\end{aligned} \tag{A1.5}$$

Whereas all strain functions give the exact solution for a single inclusion in an infinite medium, the problem of interacting inhomogeneities leads to approximate solutions because the strains induced by a $\boldsymbol{\beta}_j^p(a,b,c)$ distribution cannot be exactly expressed by a Taylor series with a finite T value at every point. Therefore, the equality between the stress inside an inhomogeneity p and that inside the corresponding equivalent inclusion, which induces an eigenstrain, is rewritten in the form:

$$\begin{aligned}
&\sum_{j=1}^{6}\mathbf{C}_{ij}^p\Bigg(\boldsymbol{\epsilon}_j^{0p}(a,b,c) + \sum_{k=1}^{6}\sum_{q=1}^{N}\sum_{a',b',c'}^{0\leq a'+b'+c'\leq T} \\
&\quad \times \mathbf{D}_{jk}^{pq}(a,b,c,a',b',c')\boldsymbol{\beta}_k^q(a',b',c')\Bigg) \\
&= \sum_{j=1}^{6}\mathbf{C}_{ij}^0\Bigg(\boldsymbol{\epsilon}_j^{0p}(a,b,c) + \sum_{k=1}^{6}\sum_{q=1}^{N}\sum_{a',b',c'}^{0\leq a'+b'+c'\leq T} \\
&\quad \times \mathbf{D}_{jk}^{pq}(a,b,c,a',b',c')\boldsymbol{\beta}_k^q(a',b',c') - \boldsymbol{\beta}_j^p(a,b,c)\Bigg)
\end{aligned} \tag{A1.6}$$

for all (a, b, c) and for every i and p. The compliance tensors are assumed to be uniform. The $\boldsymbol{\beta}_j^p(a,b,c)$ are the initial unknowns and Eq. (A1.6) gives an approximate solution of the mechanical interaction problem. The number of unknowns per inhomogeneity is 6 for a truncation order T of zero, 24 for $T=1$, 60 for $T=2$, 120 for $T=3,\ldots$

At this stage, it should be noted that the left hand side of Eq. (A1.4), the heterogeneous problem, involves non-equilibrated stress fields, while the right hand side, the homogeneous equivalent problem, deals with equilibrated stress fields. The right hand side of this equation is in fact the sum of exact solutions for the inclusion problem. Since $\mathbf{C}^p \neq \mathbf{C}^0$, the left hand side generally involves non-equilibrated stress fields due to the normal stress discontinuities at the interface and non-zero body forces which remain for truncated Taylor series. Considering now Eq. (A1.6), the left hand side concerns non-equilibrated stress fields for the same two reasons, while on the right hand side the estimation of $\mathbf{D}$ by truncated Taylor series also mostly leads to non-equilibrated stress fields. The exact solution is obtained when the stress field on the left hand side is equilibrated.

Since the present computations were applied to isotropic materials, the $\mathbf{C}_{ij}$ tensors depend only on the shear and bulk moduli. It should be noticed that the particular case of cavities ($\mu = k = 0$), Eq. (A1.6) has no single solution due to the vanishing right hand term and therefore leads to 'impotent eigenstrains'. It is nevertheless possible to derive specific equations for cavities. A simple way of avoiding numerical problems without restricting the potential of our software was adopted here: the elastic constants of the cavities were set to 10^{-6} times those of the matrix. Computing with double precision reals makes the error introduced by this simplification negligible compared to that resulting from truncation of the Taylor series.

A.2. Quality of the solution

The solution given by the EIM Eq. (A1.6) is kinematically admissible, accounts for the behaviour of the material and fulfils the boundary conditions, but it is not statically admissible for the following reasons. A polynomial eigenstrain of degree N induces a polynomial eigenstrain of the same degree inside an inclusion. Therefore, any polynomial applied strain can be exactly counterbalanced by polynomial eigenstrains in the equivalence equation. In contrast, the eigenstrains outside the inclusion, which vanish at infinity, involve functions of the type $x^a\ y^b\ z^c\ (\sqrt[2]{x^2+y^2+z^2})^n$ where $n \leq -(a+b+c+3)$, and such terms cannot be exactly counterbalanced by a truncated Taylor series. These 'external' strains act as applied strains arising from the surrounding interacting inhomogeneities. Two quantities based on the amplitude of the stress discontinuities and of the self induced body forces, calculated from the left hand side of Eq. (A1.4) have been proposed in Ref. [13] to assess the quality of the solution. The first one is

based on the stress jump at the inhomogeneity interface and presented below. The second one is based on the equilibrium related to parasitic body forces, related to the approximation of Eq. (A1.6), inside the inhomogeneity. Since the latter is not useful for voids or rubber particles for which the inner stress fields tend to be uniform, it is not detailed herein.

The strain field induced by a eigenstrain $\boldsymbol{\beta}_j^p(a,b,c)$ in a domain Ω_p is continuous across the interface with another domain Ω_q. The approximate solution follows the stress gradients as well as possible by means of terms varying with a Taylor expansion around the centre r_q of Ω_q, i.e. a sum of terms $x^{a'}\ y^{b'}\ z^{c'}$. Although all terms are then correctly counterbalanced at the centre of an inhomogeneity, stress discontinuities σ_i^{dis} are expected to appear at the interface:

$$\sigma_i^{\mathrm{dis}} = \sigma_i^{+} - \sigma_i^{-} \tag{A1.7}$$

where σ_i^{+} and σ_i^{-} denote the components of the stress tensor at the external and internal faces, respectively, corresponding to the left hand side of Eq. (A1.4). These discontinuities clearly increase as the distances between inhomogeneities decrease and as the difference between the material elastic constants ($\mathbf{C}^p - \mathbf{C}$) increases. Therefore, a quantity J_q derived from the stress discontinuities provides an estimate of the quality of the approximate solution. At the interface of a given inhomogeneity q, we propose to use a positive mean value based on the amplitude of the stress discontinuity. Since σ_i^{dis} increases with $\mathbf{C}_{ij}^p - \mathbf{C}_{ij}^0$, the displacement vector is employed as a normalisation weight. Denoting by $\mathbf{u}_q$ the displacement vector at the centre of the inhomogeneity q of radius a_q, J_q is defined by:

$$J_q = \frac{3}{4\pi a_q^3(\boldsymbol{\epsilon}^0\boldsymbol{\sigma}^0)} \int_{S_q} |(\boldsymbol{\sigma}^{\mathrm{dis}}\cdot\mathbf{n})|\cdot|(\mathbf{u}-\mathbf{u}_q)|\mathrm{d}s \tag{A1.8}$$

where $\mathbf{n}$ is the normal vector outward the interface and S_q is the surface of Ω_q. J_q is a dimensionless quantity, which is always positive and zero for the exact solution.

References

[1] Collyer A. Rubber toughened engineering plastics. London: Chapman & Hall, 1994. ISBN 0 412 58380 1.
[2] Béguelin PH, Kausch HH. J Mater Sci 1994;29:91–8.
[3] Béguelin PH. Approche Expérimentale du Comportement Mécanique des Polymères en Sollicitation Rapide. PhD Thesis Ecole Polytechnique Fédérale de Lausanne No 1572, 1996.
[4] Gensler R, Plummer CJG, Grein C, Kausch HH. Polymer 2000;41:3809–19.
[5] Dompas D, Groeninckx G. Polymer 1994;35:4743–9.
[6] Bucknall CB, Karpodinis A, Zhang XC. J Mater Sci 1994;29:3377–83.
[7] Lazzeri A, Bucknall CB. J Mater Sci 1993;28:6799–808.
[8] Schirrer R, Fond C, Lobbrecht A. J Mater Sci 1996;31:6409–22.
[9] Fond C, Schirrer R. Notes aux C.R.A.S Ser IIb 2001;5:1–6.
[10] Fond C, Lobbrecht A. Int J Fract 1996;77:141–59.
[11] Green AE, Zerna W. Theoretical elasticity. Oxford: Oxford University Press, 1954.
[12] Ball JM. Proc R Soc Lond, Ser A 1982;306:557–611.
[13] Fond C, Riccardi A, Schirrer R, Montheillet F. Eur J Mech A/Sol 2001;20:59–75.
[14] Eshelby JD. Proc R Soc Lond, Ser A 1957;241:376–96.
[15] Eshelby JD. Proc R Soc Lond, Ser A 1959;252:561–9.
[16] Moschovidis ZA, Mura T. J Appl Mech, Trans ASME 1975:847–52.
[17] Mura T. Micromechanics of defects in solids. 2nd ed. Dordrecht: Kluwer Academic Publishers, 1993.
[18] Press WH, Teukolsky S, Vetterling WT, Flannery BP. Numerical recipies — Fortran version. 1st ed. Cambridge: Cambridge University Press, 1989. p. 195. ISBN 0 521 38330 7.
[19] Hashin Z, Shtrikman S. J Mech Phys Solids 1962;10:335–42.
[20] Hashin Z, Shtrikman S. J Mech Phys Solids 1962;10:343–52.
[21] Cheng C, Hiltner A, Baer E, Soskey PR, Mylonakis SG. J Mater Sci 1995;30:587–95.
[22] Fond C. Endommagement des Polymères Choc: Modélisation Micromécanique et Comportements à la Rupture, Mémoire d'Habilitation à Diriger des Recherches Université Louis Pasteur de Strasbourg, 2000.
[23] Moulinec H, Suquet P. Comput Meth Appl Mech Engng 1998;157:69–94.